Computational Particle Mechanics (2021) 8:1033–1045
https://doi.org/10.1007/s40571-020-00379-6

Investigation of the grain breakage behaviour of 2D granular materials with disordered pore distribution

Quanshui Huang[1] · Wei Zhou[1] · Gang Ma[1] · Jiangzhou Mei[1] · Kun Xu[2,3]

Received: 10 November 2019 / Revised: 3 November 2020 / Accepted: 19 November 2020 / Published online: 3 January 2021

Abstract
Granular materials have been widely used in the field of geotechnical engineering. Being one of the intrinsic properties of granular materials, the internal grain porosity greatly affects their mechanical properties, grain crushing in particular. In this article, the single porous grains with different degrees of disordered pore distribution were generated and fully investigated with discrete element method (DEM). The degree of disorder of pore distribution is characterized by parameter I_v. The DEM results demonstrate that both number of pore and the disorder of pore distribution have great effects on crushing strength. A more disordered pore distribution could lead to higher stress concentration and the heterogeneity of stress distribution, which results in a lower crushing strength. The shape of remaining fragments after grain crushing shows that the cracking path becomes more irregular with increasing disorder of pore distribution. For the three studied porosity, the crushing strength complies with an exponential-law diminution with the increase in disorder degree of pore distribution. The grain crushing strength was also statistically analysed by Weibull distribution. Similar to crushing strength, the Weibull modulus, m, of grain crushing strength follows an exponential law, in other words, m decreases with the disorder degree of porous texture. These results deepen our understanding of the effect of pore disorder over crushing behaviour of granular matter.

Keywords Discrete element method · Grain breakage · Porous material · Weibull statistics · Disordered pore distribution

1 Introduction

Granular materials are commonly utilized in geotechnical engineering, including rock-fill dam, railway, mining and so on [1–9]. The mechanical properties of granular material, such as deformation, strength and grain crushing, are very complicated and random due to its complex internal structure (mineral composition, flaw and pore) and external factor (size, shape and environment effect) [10, 11]. Recently, the study of multi-pore behaviour has become an important issue as tailoring porous texture is a potential approach of controlling macroscopic properties of brittle materials [12]. For this reason, the mechanical properties (especially grain crushing) of granular materials under multi-pore impact should also be further studied.

According to previous studies, the porosity of different types of rocks vary greatly [13–17], in addition, pore size and geometry are also unique for each type. Yang et al. [18] experimentally investigated strength, deformation and crack evolution behaviour of sandstone, whose porosity was 6.88%. In their study, the micropores of tested sandstone were shown by scanning electron microscopy (SEM) image. Zhang et al. [19] found evidence of internal voids in grains that were in contact with surface via the photograph of soil particles with size 0.6–1.18 mm before testing. Al-Harthi et al. [20] presented a photograph of tested vesicular basalt revealing the variation in the size of non-connected pore spaces. In their research, an image analysis technique was suggested to estimate the porosity of vesicular basalt.

✉ Wei Zhou
zw_mxx@whu.edu.cn

[1] State Key Laboratory of Water Resources and Hydropower Engineering Science, Wuhan University, Wuhan 430072, Hubei, China

[2] Changjiang Institute of Survey, Planning, Design and Research, Wuhan 430010, Hubei, China

[3] Key Laboratory of Failure Mechanism and Safety Control Techniques of Earth-Rock Dam of the Ministry of Water Resources, Nanjing 210024, Jiangsu, China

Numerical simulation methods, including discrete element method (DEM), combined finite-discrete element method (FDEM), lattice element method (LEM), are useful tools for obtaining micro-mechanical information and have been extensively employed to study the mechanical behaviour of brittle porous materials [21–27]. Fakhimi et al. [28] studied the effects of porosity and pore size on rock deformational and strength characteristics employing a bonded particle model. Their results demonstrate that apart from porosity, pore size could induce drastic change in elastic modulus, crack initiation stress and rock strength. Nguyen et al. [29] numerically investigated the influences of pore structure over fracture behaviour of geopolymer-foamed concrete and found that pore size could produce dramatic effect on fracture resistance. They also discovered that a decrease in pore size resulted in higher compressive strength and this phenomenon is more significant for foam concrete with lower porosity. Cui et al. [30] performed a micro-mechanical study using lattice spring model (LSM) and found out that porosity had a significant impact on fracture strength while pore size dominated the Weibull modulus. Laubie et al. [12] investigated the stress transmission of a brittle porous material and its relation with failure properties by conducting a lot of lattice-element simulations. The authors observed a non-Gaussian broadening of stress probability density functions under tensile loading, which is caused by disordered pore distribution.

In this work, based on DEM, a series of simulations were conducted to investigate the influences of porosity and disorder of pore distribution on single grain crushing. The single grain model was generated by means of bonded particle model, in which elementary particles were cemented by removable bonds. The single grain models with various porosity were achieved by deleting different number of particles. The disorder degree of pore distribution is defined by parameter I_v. The results of grain crushing strength, fracture and fragmentation patterns, and the like, offer insight into the influence of porous disorder over mechanical properties of granular porous materials.

2 Single porous model and its calibration

2.1 Generation of disordered pore distribution

The 2D-DEM model adopted in current simulations is shown in Fig. 1, in which the single grain was modelled as an agglomerate of elementary particles with removable bonds. The radii of single grain (r_g) and elementary particles (r) are 30 and 0.3 mm, respectively. The number of elementary particles is 9366. It should be noted that the packing structure of elementary particles is regularly hexagonal; in this case, the strength of grain model is statistically homogeneous. For such an entirely regular DEM agglomerate, its theoretical porosity (i.e. the ratio of blue area to red triangle area in Fig. 2) is given by:

$$\varphi = S_1/S_2 = 1 - \sqrt{3}\pi \Big/ 6 \approx 0.0931 \tag{1}$$

where S_1 and S_2 are the area of blue and red triangle area, respectively.

In this study, additional porosity was introduced into the grain model presented above by removing a certain number of particles. A strategy of generating porous agglomerates with controlled disordered degree is presented as follows. As illustrated in Fig. 3, the grain was virtually discretized by a lot of cells, resultant nodes were used as reference position for removing particles. The shape of cell is square, and the width l of cell determines the number of nodes that fall within the grain boundary. Considering a concentric circular area with a radius of $(r_g - l)$ as a boundary, node that falls into this area should be considered for deleting particles. One particle is randomly removed within a certain distance R from each node. The uniform reference distance, R, for each case should be specified according to the degree of disorder of the pore distribution. As revealed from Fig. 3a, a bigger boundary means the scope for deleting particles expands accordingly. In this generation strategy, the number of nodes located within $(r_g - l)$ of the grain centre equals to the number of deleted particles n, as a result, the porosity can be calculated by:

$$\varphi = \varphi_0 + n\left(r/r_g\right)^2 \tag{2}$$

The degree of disorder of pore distribution is calculated by:

$$I_v = \delta/l \tag{3}$$

By adopting the aforementioned approach, samples with different porosity are able to be generated with regard to the same reference grid, furthermore, corresponding degree of disorder for these samples could be controlled by varying δ. As listed in Table 1, a wide range of variation in porosity is considered, but only the highly ordered ($I_v = 0$) and disordered ($I_v = 2.0$) pore distribution are considered for Case-1; while for Case-2 to Case-4, eight kinds of degree of pore disorder (from $I_v = 0$ to $I_v = 2.0$) are investigated. Thirty simulations (referred to as a group) will be performed for each porosity and pore disorder by setting different seeds adopted in random-number generator. Therefore, a total of 54 groups of grain crushing tests will be simulated in this study. Three samples with the same porosity (Case-2) but increasing porous disorder are shown in Fig. 4. For the highly ordered system, i.e. $I_v = 0$, small fluctuations in pore distribution still exist as it is not always possible to find the particle exactly at cell node

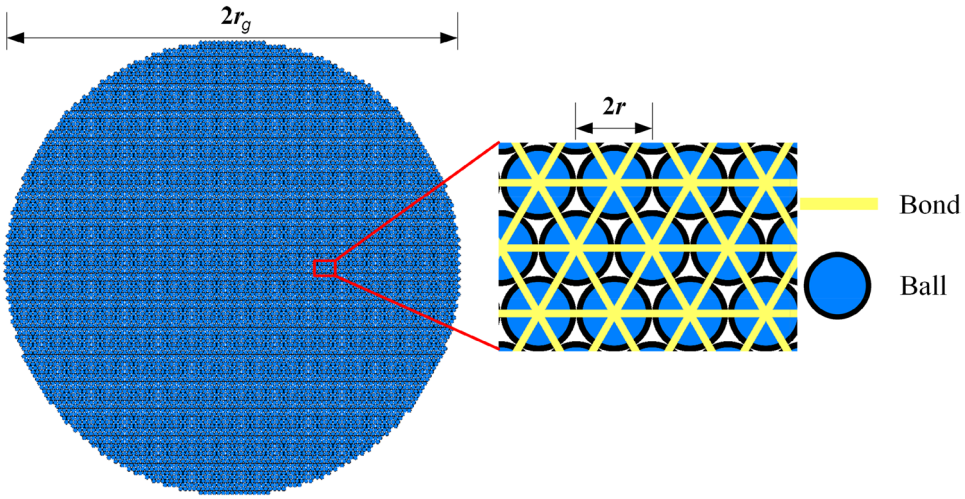

Fig. 1 Initial single grain model and its packing structure

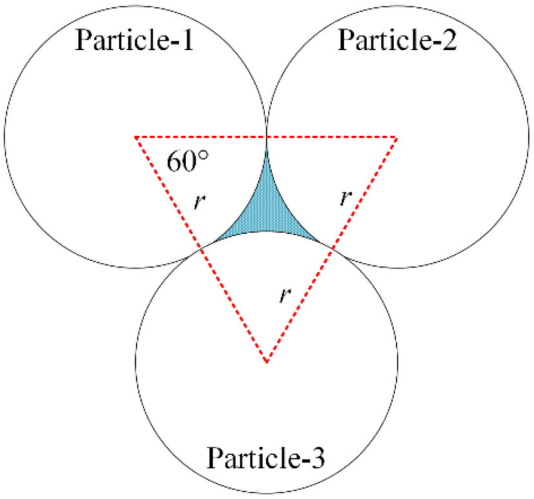

Fig. 2 Schematic diagram for calculating theoretical porosity. r is the radius of elementary particles, equalling to 0.3 mm here

position to delete. Figure 5 displays grains with the same porous disorder (I_v = 2.0) but with increasing porosity.

2.2 Porous disorder calibration

As described method of removing particles above, the parameter I_v of pore disorder is a predetermined quantity, other geometrical descriptors are needed in order to verify whether the generated grain models meet requirements of different disorder. Here, another disorder parameter I_d is defined to calibrate the aforementioned porous grain models. In the first step, the centres of removed particles were connected to form a triangular grid according to principle of nearest distance, as shown in Fig. 6. Secondly, the area of each triangle mesh will be calculated and the standard deviation of the triangular area is given as:

$$\mathrm{SD} = \sqrt{\frac{1}{n}\sum_{i=1}^{n}\left(S_i - \overline{S}\right)^2} \tag{4}$$

where n is the number of triangular grid, S_i is the area of triangular grid i, $\overline{S}$ is the average area of triangular grids.

And then the disorder parameter I_d is defined as:

$$I_\mathrm{d} = \mathrm{SD}/\left(l^2/2\right) \tag{5}$$

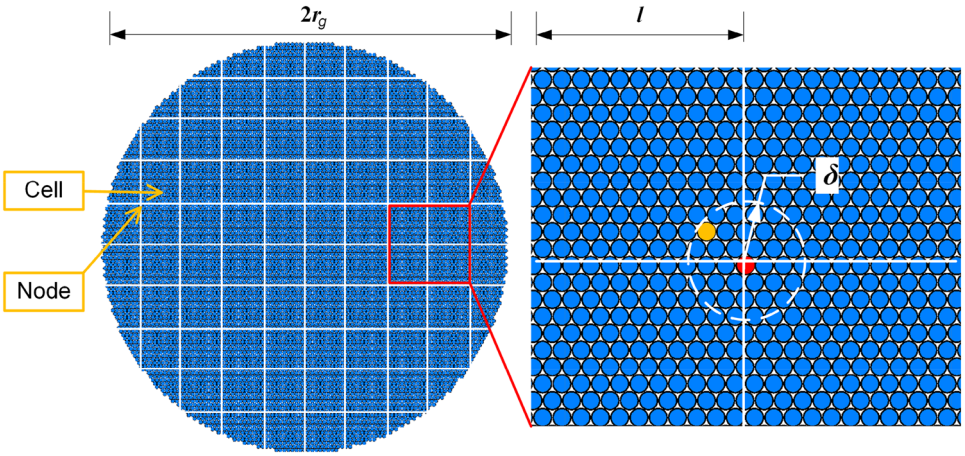

Fig. 3 The reference grid used for removing particles

Table 1 Calculation scheme

Case	Cell side length l (mm)	Number of pores n	Porosity φ	Pore disorder I_v
1	From 6.0 to 1.0	From 57 to 2669	From 0.0988 to 0.360	0.0 (a total of 18 groups)
				2.0 (a total of 18 groups)
2	3.0	261	0.119	0.0
				0.2
				0.4
3	2.0	628	0.156	0.6
				0.8
				1.0
4	1.5	1148	0.208	1.25
				1.5
				2.0

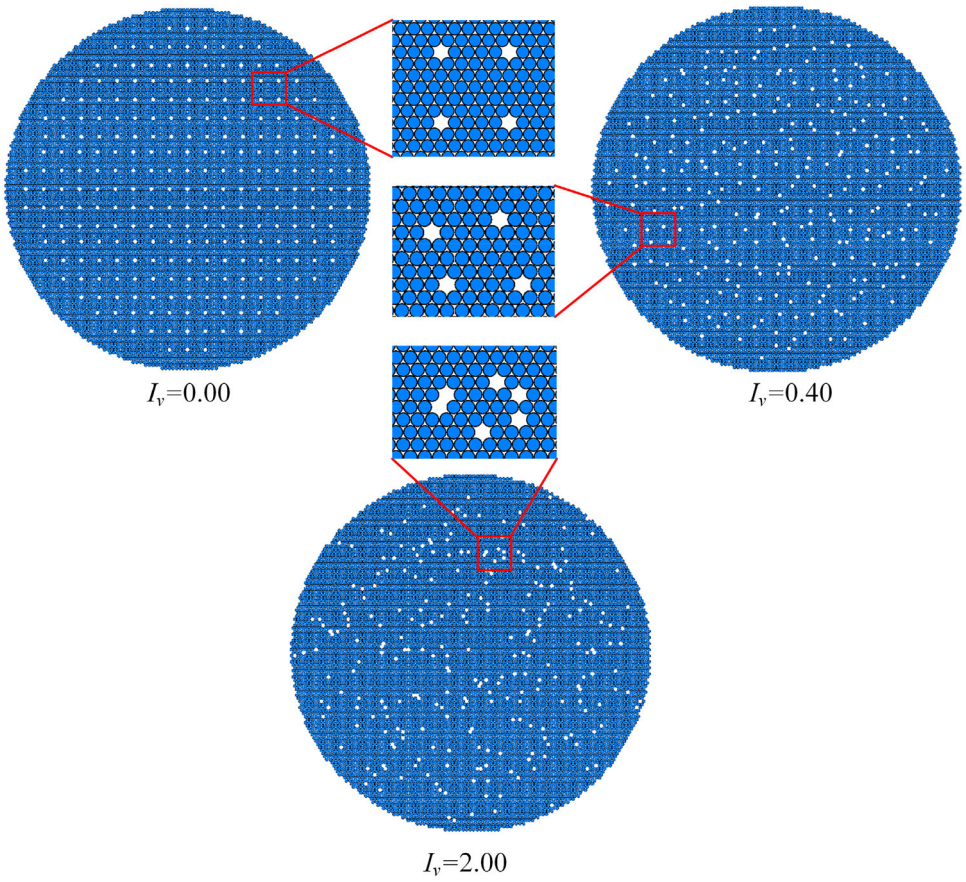

Fig. 4 DEM samples with the same porosity but different porous disorder degree (Case-2)

As illustrated in Fig. 6b, I_d increases with I_v, which confirms that porous structures with different disorder degree could be generated via proposed approach. Note that the nonlinear relationship between I_d and I_v reveals that the degree of disorder of the pore distribution plateaus after a certain growth with I_v. The ceiling of I_d is achieved in the case of completely random pore generation.

3 Numerical simulation grain crushing test and relevant parameters

The DEM simulation of the single grain crushing test was carried out using PFC^{2D} [31]. The top and bottom rigid walls were generated at the top and bottom of the agglomerate, respectively. The agglomerate was then crushed by moving the top loading wall downwards. As for the loading speed, as shown in Fig. 7, if loading becomes too fast, the peak force would be large and the displacement

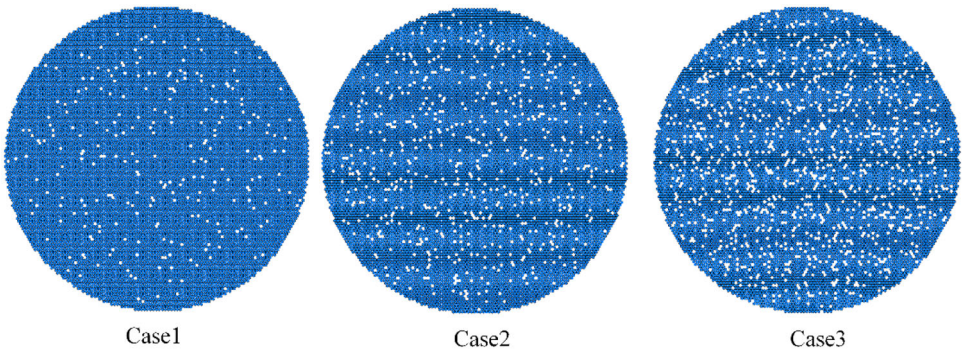

Fig. 5 DEM samples with the same porous disorder degree (I_v = 2.0) but different porosity

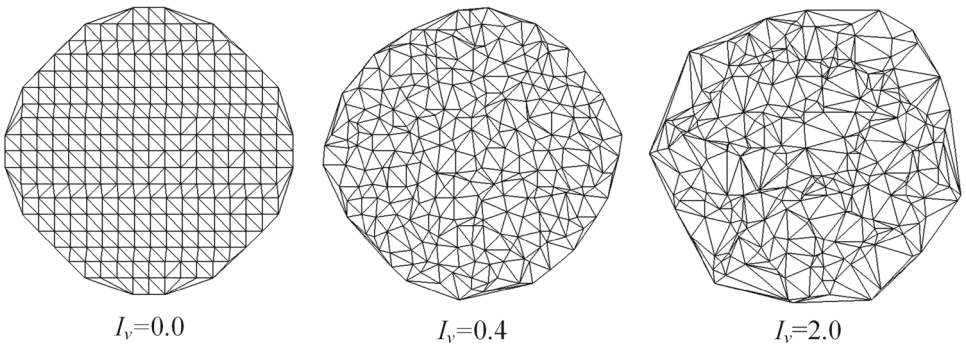

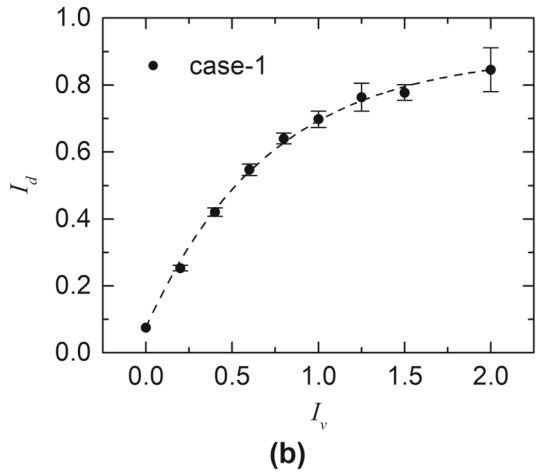

Fig. 6 **a** Triangular mesh formed by deleted particles; **b** validation of I_v via I_d

corresponding to peak force would exceed the threshold of the static state. Therefore, the loading velocity was set to 0.001 m/s which is small enough to ensure quasi-static condition and to avoid the occurrence of dynamic response. During the loading process, the loading force acting on the rigid wall, F, and displacement of the top wall, S, were recorded in each step. In addition, the maximum value of the recorded loading force was defined as the maximum force, $F_{\max}$. The compression was terminated when the force acting on the rigid wall was less than 0.6 $F_{\max}$.

The DEM input parameters listed in Table 2 were calibrated by a trial and error process (refer to the author's previous research [32]) to guarantee the occurrence of brittle failure during grain crushing process, in other words, the material will have little plasticity to resist the propagation of the crack and the material fails by fast fracture. To be more specific, the ratio of wall displacement for bulk failure of grains to grain diameters should be less than 0.3%.

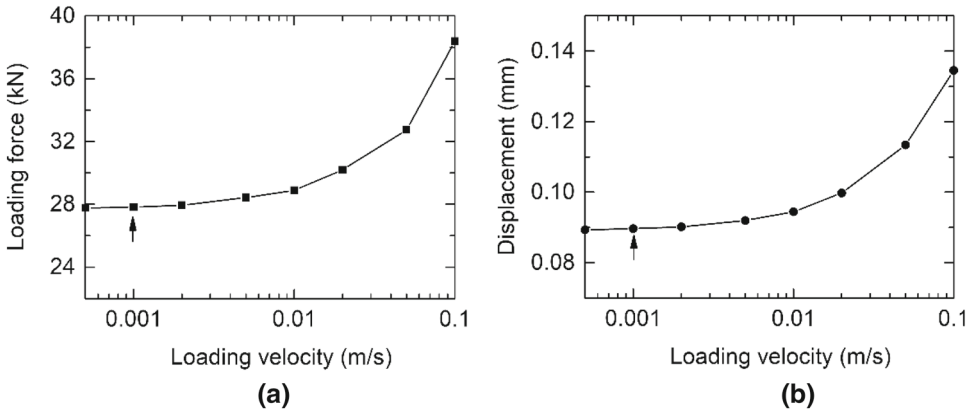

Fig. 7 **a** Peak force as a function of loading velocity, **b** displacement corresponding to peak force as a function of loading velocity

Table 2 DEM parameters of the elementary particles, parallel bonds and boundary walls

PFC elements	Description	Parameter	Value
Elementary particles	Particle radius (mm)	r	0.3
	Density (kg/m^3)	ρ	2706
	Local damping coefficient	β_{ball}	0.7
Linear contact model	Effective modulus (GPa)	E_{linear}	0.4
	Normal-to-shear stiffness ratio	$k_{\text{n-linear}}/k_{\text{s-linear}}$	2.5
	Normal and shear critical damping ratio	$\beta_{\text{n}}/\beta_{\text{s}}$	0.5
	Friction coefficient of the wall	u	0.7
Parallel bonds	Effective modulus (GPa)	E_{pb}	0.4
	Normal-to-shear stiffness ratio	$k_{\text{n-pb}}/k_{\text{s-pb}}$	2.5
	Tensile strength (MPa)	σ_c	0.5
	Cohesion (MPa)	c	0.5
	Friction angle (degrees)	ϕ	30°
Walls	Normal stiffness (N/m)	$k_{\text{n-wall}}$	1e9
	Shear stiffness (N/m)	$k_{\text{s-wall}}$	5e7
	Friction coefficient	u_{wall}	0.25

4 Results

4.1 Influence of porous disorder on stress field and fracture patterns

It is generally believed that the existence of pores is expected to affect the stress transmission and lead to stress concentration. In addition, the pore distribution is able to exert an influence over degree of stress concentration. In order to display stress distribution inside the grain, the stress tensor resulted from all contacts force acting on each ball is computed by Eq. (6) [33].

$$\sigma_{ij} = \frac{1}{V}\sum_{c=1}^{M} f_j^{(c)} L_i^{(c)}, \tag{6}$$

where V is the volume of a region; M is the number of contacts on the boundary; $f_j^{(c)}$ is contact force vector; $L_i^{(c)}$ is the vector connecting the centre of the two contiguous balls. It should be noted that the compressive stress is negative by default.

Four contour plots of X tensile stress (σ_{xx}) are shown in Fig. 8 for samples with the same porosity $\varphi = 0.101$ but incremental disorder when loading force equals 15 kN. The region of local stress concentration is denoted as red spots. Revealed from Fig. 8a–d, the tensile stress is mainly distributed on the central axis of grain, which is consistent with the published research [34]. Furthermore, the local stress concentration inside grain grows with the degree of disorder of pore distribution. Higher stress concentration and its heterogeneity would result in a lower particle crushing strength.

The aforementioned stress distribution inside the grain directly affects the mechanical behaviour of grain sample, especially the stress–strain curve. In general, the characteristic tensile stress induced in a 2-D grain under compression is defined as [35], $\sigma = \frac{F}{d}$, where F and d refer to diametrical force and distance between two platens at failure under compression, respectively. In addition, the

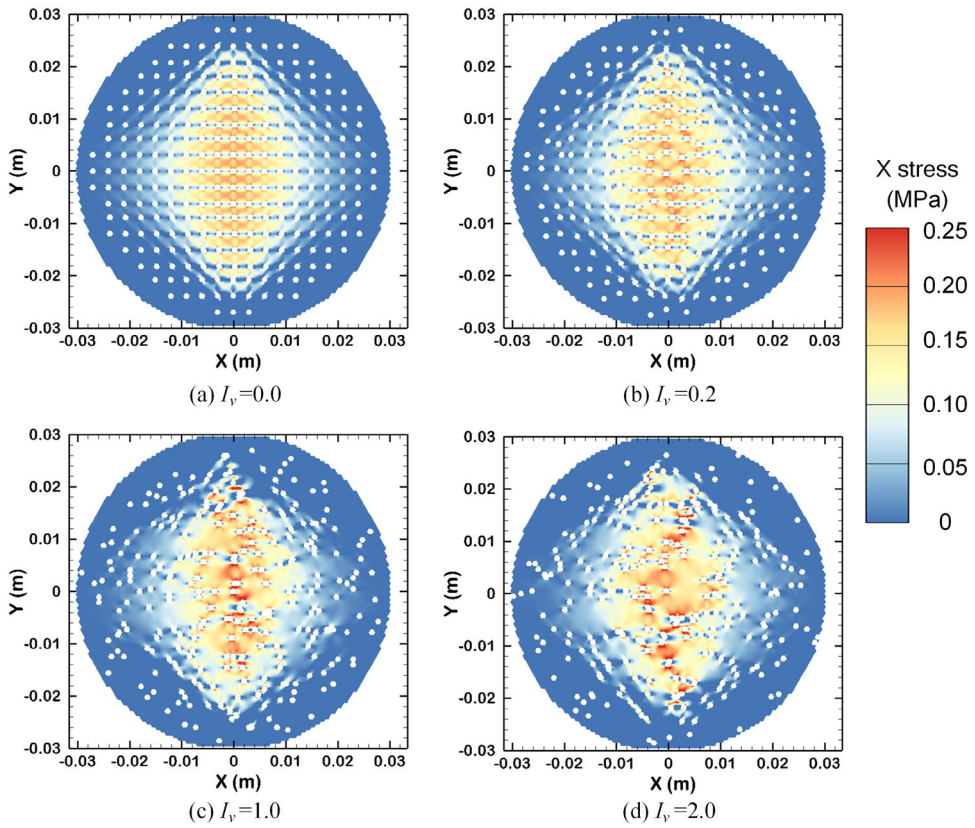

Fig. 8 *X* tensile stress field in four different samples of incremental disorders (Case-2). The wall loading force equals 15 kN

vertical strain is given by, $\varepsilon = s/d$, where s is the vertical displacement of loading wall. Figure 9a exhibits four curves of stress–strain behaviour for grain samples with the same porosity but different porous disorder during compression. The peak stress (i.e. grain crushing strength) is maximum for model with disorder $I_v = 0$ while the model with disorder $I_v = 2.0$ has the lowest peak stress. For high-disorder sample, the force–displacement curve demonstrates a little fluctuation prior to reaching peak stress, indicating that the damage incepts inside the grain under a certain external load. In order to further discover a universal link between stress distribution inside grain and vertical peak stress, the vertical stress is normalized by weighted internal stress corresponding to peak stress (see Fig. 9b). It is found out that all four curves reach almost the same peak value, which illustrates that the internal stress distribution induced by porous disorder determines the crushing strength. Or rather, the more obvious stress concentration is, the lower the crushing strength becomes.

By and large, the initiation and propagation of fracture in terms of brittle material appear in areas where stress exceeds the strength threshold. As a result, changing

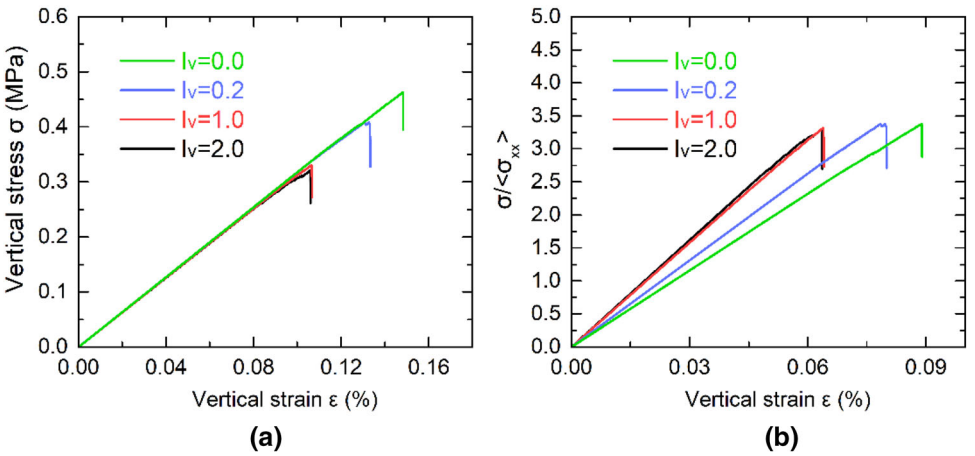

Fig. 9 **a** Vertical stress versus vertical strain for different pore disorders (Case-2). **b** Vertical stress normalized by weighted internal stress corresponding to peak stress versus vertical strain for different pore disorders (Case-2)

degree of inhomogeneity of stress distribution could give rise to diverse fracture patterns. Figure 10 displays snapshots of four cracking grains with different disorder degree of porous textures. Under the four scenarios, main cracks all propagate vertically and have contact with both top and bottom walls; however, deviations from the vertical axis become larger from Fig. 10a–d, which signifies that porous disorder plays a critical role in fracture progression. The progressively uneven pattern of fracture path also demonstrates that remaining fragments after grain crushing are more irregular as the degree of porous disorder rises.

4.2 Influence of porous disorder on grain crushing strength

As mentioned in Sect. 4.1, the degree of stress concentration inside the grain increases with the disorder of porous texture; in this case, the crushing strength of grain is variable according to its disorder of porous structure. As illustrated in Fig. 11, the average grain crushing strength of 54 groups (as listed in Table 1) is well correlated with both porosity and pore disorder. For Case-1 when I_v equals 0,

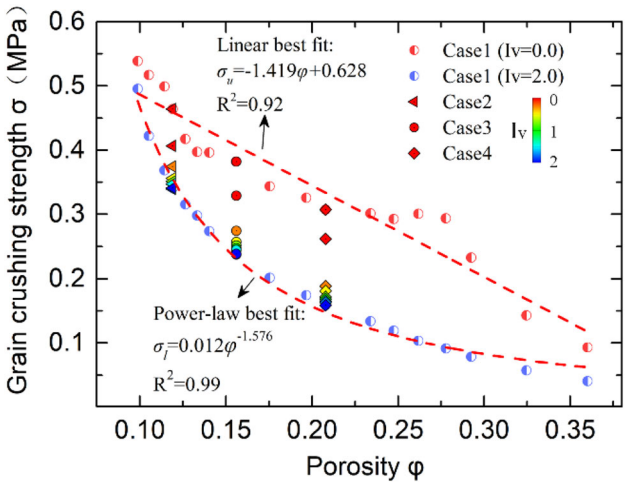

Fig. 11 Grain crushing strength, σ, as a function of porosity, φ

Fig. 10 Influence of porous disorder on fracture pattern (Case-2)

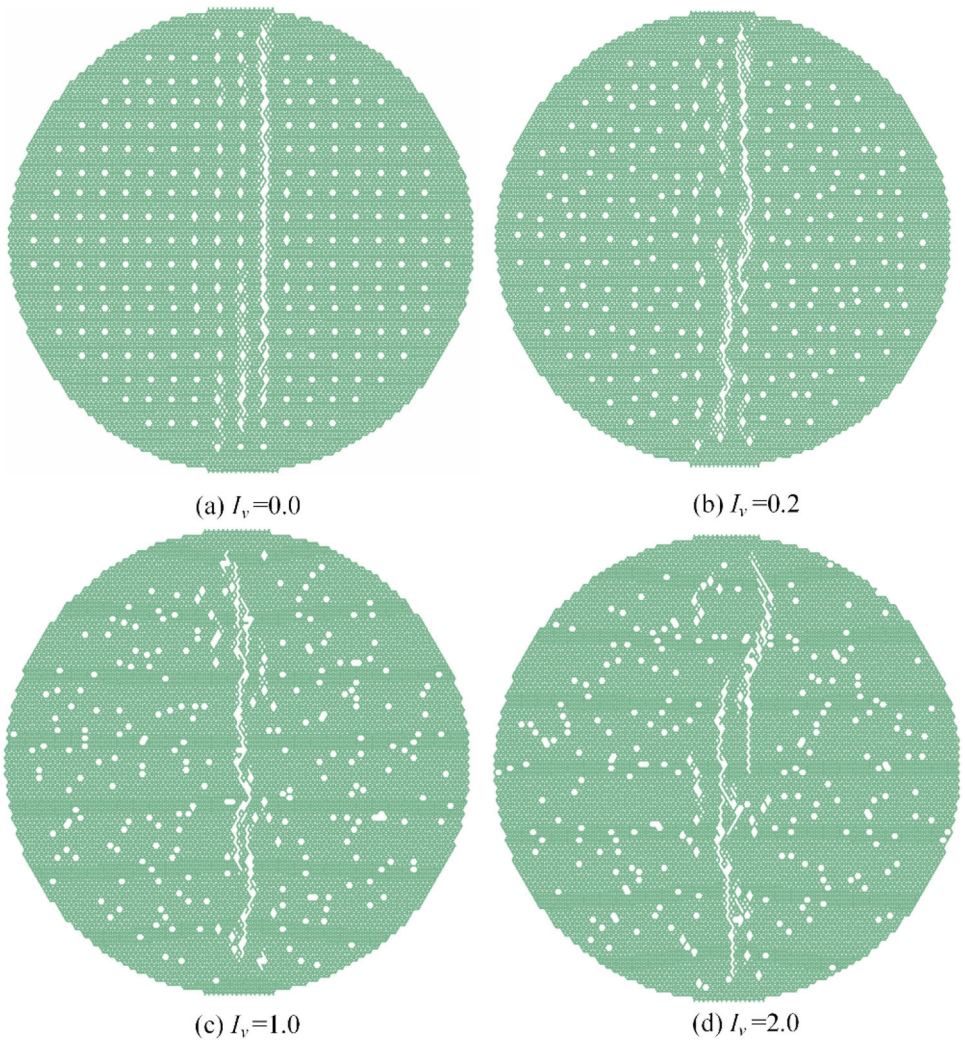

the crushing strength presents an overall linear downward trend with increasing porosity, which is fitted by:

$$\sigma_u = -1.419\varphi + 0.628 \tag{6}$$

While for Case-1 when I_v equals 2, the crushing strength exhibits an overall power-law downward tendency with porosity, fitted by:

$$\sigma_l = 0.012 \times \varphi^{-1.576} \tag{7}$$

For Case-2, Case-3 and Case-4, to better understand the relationship between grain crushing strength and pore disorder, σ versus I_v for three cases with different porosity are plotted in Fig. 12. The error bars are the standard deviations of crushing strength of 30 grains in each group. In Fig. 12, the uniform expression for exponential best fit curves is given as Eq. (8).

$$\sigma = \sigma_1 + A \times \exp(B \times I_v) \tag{8}$$

where σ_1 is the strength value when $I_v \to \infty$, $A + \sigma_1$ denotes the initial value when I_v is 0, B refers to the rate of curve.

Furthermore, the curves displayed in Fig. 12a–c were normalized by crushing strength when pore disorder is zero. As illustrated in Fig. 12d, curves for three cases with different porosity diverge with the same starting point. For Case-4, the vertical decrease is maximum. This can be further explained that when porosity is large, stress concentration caused by the same disorder is greater than that caused by low porosity.

4.3 Influence of porous disorder on strength variability

It has been theoretically and experimentally validated that grain crushing strength follows a Weibull distribution [32, 36–42]. As demonstrated by Mcdowell and Amon [36], the survival probability for a grain with size d under diametrical compression is given by:

$$P_s(d) = \exp\left[-\left(\frac{d}{d_0}\right)^3 \left(\frac{\sigma}{\sigma_0}\right)^m\right] \tag{9}$$

where m is the Weibull modulus, d_0 denotes a reference size and σ_0 represents the characteristic stress for a grain of size, d_0, based on the assumption that 37% of the tested grains survive.

As to experiment using finite number of grains, the survival probability,P_s, is calculated on the basis of mean rank order:

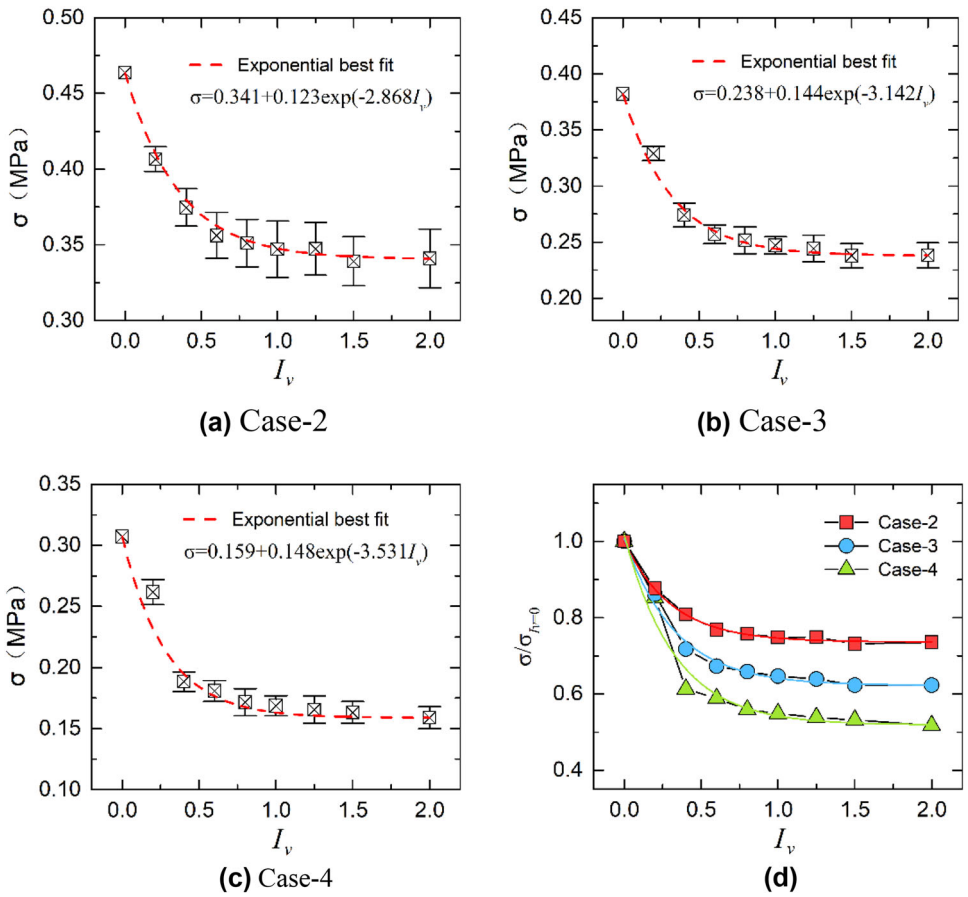

Fig. 12 **a–c** Crushing strength versus I_v for three cases. **d** The crushing strength for Case 2–Case 4 normalized by strength when $I_v = 0$

$$P_s = 1 - \frac{i}{N+1} \tag{10}$$

where N is the total number of grains, and i is the rank of the grain arranged in ascending order. Therefore, for a group of 30 grains, the grain failing at the lowest value of σ has a survival probability of 1/31, and the strongest grain has a survival probability of 30/31.

Substituting $d = d_0$ into Eq. (9), a linear equation can be obtained:

$$\ln[\ln(1/P_s)] = m \ln \sigma - m \ln \sigma_0 \tag{11}$$

In accordance with Eq. (11), by plotting $\ln[\ln(1/P_s)]$ against $\ln \sigma$, the Weibull modulus, m, could be determined from the slope of the line of best fit, while σ_0 is the value of σ when $\ln[\ln(1/P_s)] = 0$, denoted as characteristic strength. The simulation data of four groups for Case-2 and corresponding Weibull best fitting curves are shown in Fig. 13a. Despite slight discrepancy, the simulation data are properly fitted by the Weibull function. When I_v approaches 0, the material is considered highly ordered. In other words, the pores are evenly distributed throughout the material; hence, there is little variability in the crushing strength. The Weibull modulus, m, decreases dramatically with pore disorder, I_v. Figure 13b demonstrates the Weibull modulus, m, as a function of disorder degree,I_v, obeys an exponential law. Figure 13c shows the characteristic strength σ_0 as a function of disorder degree, I_v, for Case-2. As for the law of characteristic strength σ_0 versus I_v, it is basically consistent with that of grain crushing strength (i.e. Fig. 12).

4.4 Influence of porous disorder on size effect of crushing strength

Since rock grains with various sizes are often encountered in geotechnical engineering, size effect of crushing strength for porous grains should be dealt carefully. In this study, the cell width, l, keeps constant while changing grain size, r_g; in addition, three different grain sizes, 20, 40 and 60 mm were considered to investigate the size effect (see Fig. 14). In view of the intractable computational burden, only four kinds of pore disorder, 0.2, 0.6, 1.25 and 2.0, along with the same porosity ($\varphi = 0.119$) were calculated and analysed as a case study.

As shown in Fig. 15a, the Weibull survival probability plots and the corresponding fitting curves for the three grain groups with different sizes are presented. It can be seen that the larger the grain size, the lower the crushing

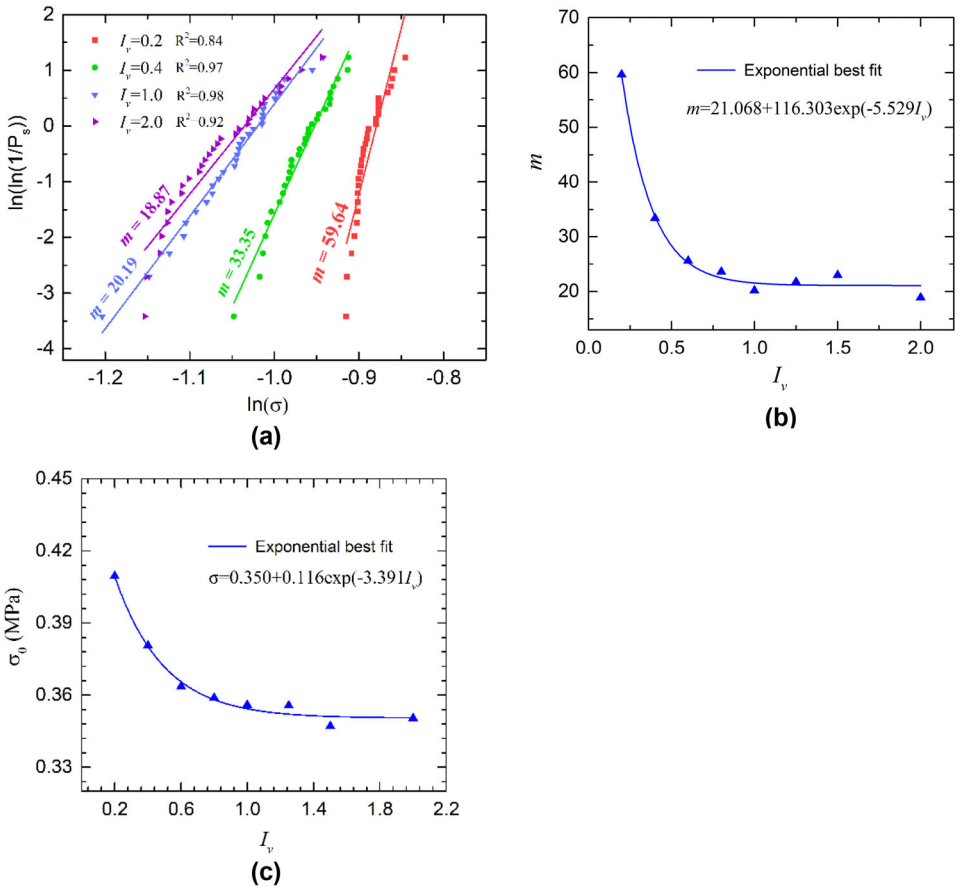

Fig. 13 **a** Weibull survival probability of the four grain groups with different disordered pore distribution (Case-2); **b** the Weibull modulus m as a function of I_v (Case-2); **c** characteristic strength σ_0 as a function of I_v (Case-2)

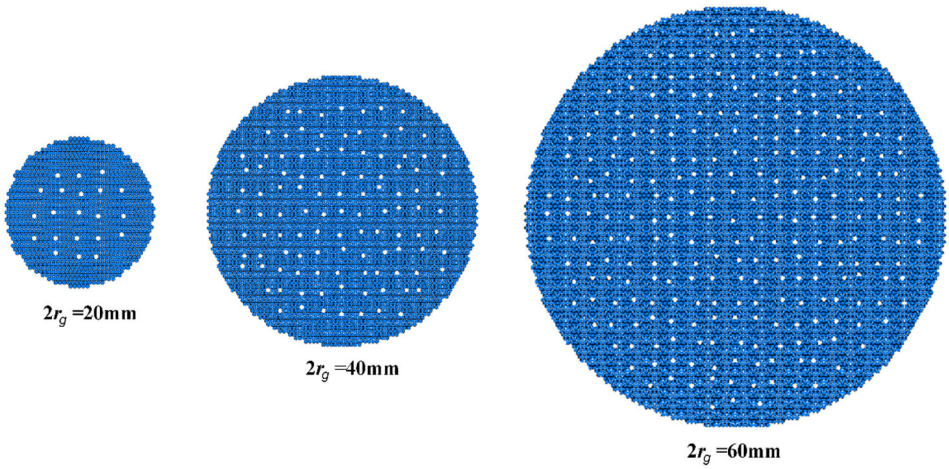

Fig. 14 DEM samples with the same porosity ($\varphi = 0.119$) and same porous disorder degree ($I_v = 0.2$) but different grain sizes

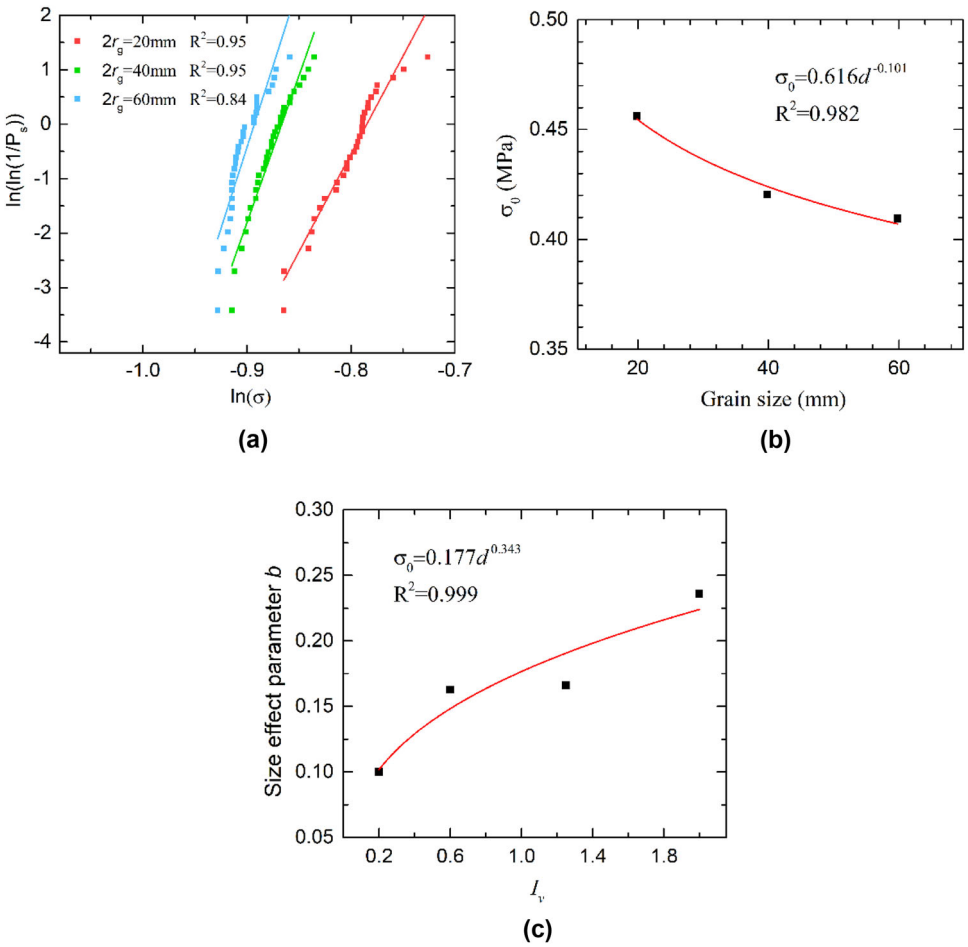

Fig. 15 **a** Weibull survival probability of the three grain groups with different sizes ($\varphi = 0.119$, $I_v = 0.2$); **b** characteristic strength σ_0 as a function of grain size ($\varphi = 0.119$, $I_v = 0.2$); **c** size effect parameter b as a function of porous disorder I_v

strength, which demonstrates the size effect of grain crushing strength. Typically, size effect of crushing strength is quantified by the following formula involving Weibull characteristic strength σ_0 and grain size d:

$$\sigma_0 = ad^b \tag{12}$$

where a and b are the fitting parameters equal to 0.616 and − 0.101 in Fig. 15b, respectively.

For different types of granular materials, the power index b varies greatly as the value of b reflects varying extent of size effect [43]. Therefore, it is necessary to study the changing pattern of size effect under the influence of pore distribution. Revealed from Fig. 15c, the parameter

b exhibits a power-law increase with the I_v, evidencing that the disorder degree of pore distribution for granular material has a significant impact on the size effect of crushing strength.

5 Conclusion

A series of simulations were carried out using DEM to investigate the influences of porosity and disorder of pore distribution over single grain crushing. The additional pores of the initial grain model are introduced by removing a certain number of elementary particles. Grain samples with the same porosity but different porous texture could be generated by varying the reference distance, δ. Furthermore, the disorder index, I_v, is devised to describe the disorder degree of porous texture. A total of 54 groups of grain crushing tests are simulated in this study, each group contains 30 grains. The effects of porous disorder on stress field, fracture patterns, crushing strength, strength variability and size effect are included in this study.

(1) The local stress concentration inside grain grows with the degree of disorder of pore distribution. Higher stress concentration and its heterogeneity would result in a lower particle crushing strength.
(2) Porous disorder is critical to fracture patterns. Deviations of main crack from the vertical axis become larger as the degree of porous disorder increases; in this context, remaining fragments after crushing become more irregular.
(3) When I_v equals 0, the crushing strength presents an overall linear downward trend with increasing porosity, while when I_v is 2, the crushing strength exhibits an overall power-law downward tendency with increasing porosity.
(4) For three kinds of porosity (Case-2, Case-3 and Case-4), the crushing strength as a function of I_v follows a uniform expression of exponential best fit curve.
(5) The simulation data of the four groups for Case-2 are properly fitted by the Weibull function. The Weibull modulus, m, decreases (obeying an exponential law) with pore disorder, I_v.
(6) The crushing strength of porous grains with different sizes exhibits obvious size effect; in addition, the size effect parameter b presents a power-law increase with the degree of disorder of pore distribution I_v.

Funding This study was funded by the National Key R&D Program of China (No. 2017YFC0404806), China Scholarship Council (Joint PhD program, No. 201906270118) and Open Research Fund of Key Laboratory of Failure Mechanism and Safety Control Techniques of Earth-Rock Dam of the Ministry of Water Resources (YK319007).

Compliance with ethical standards

Conflict of interest The authors declare that they have no conflict of interest.

References

1. Ma G, Zhou W, Chang X-L, Chen M-X (2016) A hybrid approach for modeling of breakable granular materials using combined finite-discrete element method. Granul Matter 18:7. https://doi.org/10.1007/s10035-016-0615-3
2. Zhou X, Ma G, Zhang Y (2018) Grain size and time effect on the deformation of rockfill dams: a case study on the Shuibuya CFRD. Géotechnique. https://doi.org/10.1680/jgeot.17.P.299
3. Einav I, Guillard F (2018) Tracking time with ricequakes in partially soaked brittle porous media. Sci Adv 4:1–9. https://doi.org/10.1126/sciadv.aat6961
4. Xiao Y, Liu H, Desai CS, Sun Y, Liu H (2016) Stress–strain–strength response and ductility of gravels improved by polyurethane foam adhesive. J Geotech Eng ASCE 142:06015017. https://doi.org/10.1061/(ASCE)GT.1943-5606.0001433
5. Zhou W, Ma G, Chang X-L, Duan Y (2015) Discrete modeling of rockfill materials considering the irregular shaped particles and their crushability. Eng Comput 32:1104–1120. https://doi.org/10.1108/EC-04-2014-0086
6. Wang B, Martin U, Rapp S (2017) Discrete element modeling of the single-particle crushing test for ballast stones. Comput Geotech 88:61–73. https://doi.org/10.1016/j.compgeo.2017.03.007
7. Ouhbi N, Voivret C, Perrin G, Roux J-N (2017) 3D particle shape modelling and optimization through proper orthogonal decomposition. Granul Matter 19:86. https://doi.org/10.1007/s10035-017-0771-0
8. Einav I (2007) Breakage mechanics-part I: theory. J Mech Phys Solids 55:1274–1297. https://doi.org/10.1016/j.jmps.2006.11.003
9. Ma G, Zhou W, Chang XL (2014) Modeling the particle breakage of rockfill materials with the cohesive crack model. Comput Geotech 61:1320–1143. https://doi.org/10.1016/j.compgeo.2014.05.006
10. Xiao Y, Desai CS, Daouadji A, Stuedlein AW, Liu H, Abuel-Naga H (2020) Grain crushing in geoscience materials–key issues on crushing response, measurement and modeling: review and preface. Geosci Front 11:363–374. https://doi.org/10.1016/j.gsf.2019.11.006
11. Zhou W, Ji X, Ma G, Chen Y (2019) FDEM simulation of rocks with microstructure generated by Voronoi grain-based model with particle growth. Rock Mech Rock Eng. https://doi.org/10.1007/s00603-019-02014-0
12. Laubie H, Radjai F, Pellenq R, Ulm FJ (2017a) Stress transmission and failure in disordered porous media. Phys Rev Lett 119:1–6. https://doi.org/10.1103/PhysRevLett.119.075501
13. Baud P, Wong TF, Zhu W (2014) Effects of porosity and crack density on the compressive strength of rocks. Int J Rock Mech Min Sci 67:202–211. https://doi.org/10.1016/j.ijrmms.2013.08.031
14. Wu H, Zhao J, Guo N (2018) Multiscale insights into borehole instabilities in high-porosity sandstones. J Geophys Res Solid Earth 123:3450–3473. https://doi.org/10.1029/2017JB015366
15. Cnudde V, Cwirzen A, Masschaele B, Jacobs PJS (2009) Porosity and microstructure characterization of building stones and

concretes. Eng Geol 103:76–83. https://doi.org/10.1016/j.enggeo.2008.06.014
16. Zhang W, Sun Q, Zhang Y, Xue L, Kong F (2018) Porosity and wave velocity evolution of granite after high-temperature treatment: a review. Environ Earth Sci 77:1–13. https://doi.org/10.1007/s12665-018-7514-3
17. Griffiths L, Heap MJ, Xu T, Chen CF, Baud P (2017) The influence of pore geometry and orientation on the strength and stiffness of porous rock. J Struct Geol 96:149–160. https://doi.org/10.1016/j.jsg.2017.02.006
18. Yang SQ, Huang YH, Tian WL, Zhu JB (2017) An experimental investigation on strength, deformation and crack evolution behavior of sandstone containing two oval flaws under uniaxial compression. Eng Geol 217:35–48. https://doi.org/10.1016/j.enggeo.2016.12.004
19. Zhang X, Baudet BA, Hu W, Xu Q (2017) Characterisation of the ultimate particle size distribution of uniform and gap-graded soils. Soils Found 57:603–618. https://doi.org/10.1016/j.sandf.2017.04.002
20. Al-Harthi AA, Al-Amri RM, Shehata WM (1999) The porosity and engineering properties of vesicular basalt in Saudi Arabia. Eng Geol 54:313–320. https://doi.org/10.1016/S0013-7952(99)00050-2
21. Bai QS, Tu SH, DEM Zhang C (2016) investigation of the fracture mechanism of rock disc containing hole(s) and its influence on tensile strength. Theor Appl Fract Mech 86:197–216. https://doi.org/10.1016/j.tafmec.2016.07.005
22. Gui YL, Zhao ZY, Zhang C, Ma SQ (2017) Numerical investigation of the opening effect on the mechanical behaviours in rocks under uniaxial loading using hybrid continuum-discrete element method. Comput Geotech 90:55–72. https://doi.org/10.1016/j.compgeo.2017.05.021
23. Huang YH, Yang SQ, Ranjith PG, Zhao J (2017) Strength failure behavior and crack evolution mechanism of granite containing pre-existing non-coplanar holes: experimental study and particle flow modeling. Comput Geotech 88:182–198. https://doi.org/10.1016/j.compgeo.2017.03.015
24. Ma G, Chang XL, Zhou W, Ng TT (2014) Mechanical response of rockfills in a simulated true triaxial test: a combined FDEM study. Geomech Eng 7:317–333. https://doi.org/10.12989/gae.2014.7.3.317
25. van de Steen B, Vervoort A, Napier JAL (2005) Observed and simulated fracture pattern in diametrically loaded discs of rock material. Int J Fract 131:35–52. https://doi.org/10.1007/s10704-004-3177-z
26. Hu N, Wang B, Tan GW, Yao ZH, Yuan WF (2000) Effective elastic properties of 2-D solids with circular holes: Numerical simulations. Compos Sci Technol 60:1811–1823. https://doi.org/10.1016/S0266-3538(00)00054-3
27. Zhou W, Xu K, Ma G, Chang X (2019) On the breakage function for constructing the fragment replacement modes. Particuology 44:207–217. https://doi.org/10.1016/j.partic.2018.08.006
28. Fakhimi A, Alavi Gharahbagh E (2011) Discrete element analysis of the effect of pore size and pore distribution on the mechanical behavior of rock. Int J Rock Mech Min Sci 48:77–85. https://doi.org/10.1016/j.ijrmms.2010.08.007
29. Nguyen TT, Bui HH, Ngo TD, Nguyen GD, Kreher MU, Darve F (2019) A micromechanical investigation for the effects of pore size and its distribution on geopolymer foam concrete under uniaxial compression. Eng Fract Mech 209:228–244. https://doi.org/10.1016/j.engfracmech.2019.01.033
30. Cui Z, Huang Y, Liu H (2017) Predicting the mechanical properties of brittle porous materials with various porosity and pore sizes. J Mech Behav Biomed Mater 71:10–22. https://doi.org/10.1016/j.jmbbm.2017.02.014
31. Itasca PFC3D Manual (Version 5.0). Itasca Consult. Gr. Inc.minneap (2014) www.itascacg.com/
32. Huang Q, Zhou W, Ma G, Ng TT, Xu K (2020) Experimental and numerical investigation of Weibullian behavior of grain crushing strength. Geosci Front 11:401–411. https://doi.org/10.1016/j.gsf.2019.07.007
33. Christoffersen J, Mehrabadi MM, Nemat-Nasser S (1981) A micromechanical description of granular material behavior. J Appl Mech 48:339–344. https://doi.org/10.1115/1.3157619
34. McDowell GR, Bolton MD (1998) On the micromechanics of crushable aggregates. Géotechnique 48:667–679. https://doi.org/10.1680/geot.2000.50.3.315
35. Nguyen DH, Azéma E, Sornay P, Radjai F (2015) Bonded-cell model for particle fracture. Phys Rev E Stat Nonlinear Soft Matter Phys 91:1–9. https://doi.org/10.1103/PhysRevE.91.022203
36. McDowell GR, Amon A (2000) The application of Weibull statistics to the fracture of soil particles. Soils Found 40:133–141. https://doi.org/10.3208/sandf.40.5_133
37. Ma G, Zhou W, Regueiro RA, Wang Q, Chang X (2017) Modeling the fragmentation of rock grains using computed tomography and combined FDEM. Powder Technol 308:388–397. https://doi.org/10.1016/j.powtec.2016.11.046
38. Cheng YP, Nakata Y, Bolton MD (2003) Discrete element simulation of crushable soil. Géotechnique 53:633–641. https://doi.org/10.1680/geot.2003.53.7.633
39. Cavarretta I, O'Sullivan C, Coop MR (2017) The relevance of roundness to the crushing strength of granular materials. Géotechnique 67:301–312. https://doi.org/10.1680/jgeot.15.P.226
40. Huang J, Xu S, Yi H, Hu S (2014) Size effect on the compression breakage strengths of glass particles. Powder Technol 268:86–94. https://doi.org/10.1016/j.powtec.2014.08.037
41. Xiao Y, Meng M, Daouadji A, Chen Q, Wu Z, Jiang X (2020) Effects of particle size on crushing and deformation behaviors of rockfill materials. Geosci Front 11:375–388. https://doi.org/10.1016/j.gsf.2018.10.010
42. Lim WL, McDowell GR, Collop AC (2004) The application of Weibull statistics to the strength of railway ballast. Granul Matter 6:229–237. https://doi.org/10.1007/s10035-004-0180-z
43. Hai-juan Z, Gang M, Weir Y, Wei Z, Xiao-lin C (2017) Size effect on the crushing strengths of rock particles. Rock Soil Mech 38:2425–2433. https://doi.org/10.16285/j.rsm.2017.08.032